Spatial and seasonal variations of surface ozone formation regime and source attributions in the Guanzhong Basin, China

Ruonan Wang[1,3,4], Naifang Bei[2], Jiarui Wu[1,3], Suixin Liu[1,3], Lang Liu[1,3], Xia Li[1,3], Jiaoyang Yu[1], Min Zuo[1,3], Zhenxing Shen[2], Xuexi Tie[1], and Guohui Li[1,3*]

[1]Key Lab of Aerosol Chemistry and Physics, SKLLQG, Institute of Earth Environment, Chinese Academy of Sciences, Xi'an, 710061, China

[2]School of Human Settlements and Civil Engineering, Xi'an Jiaotong University, Xi'an, 710049, China

[3]CAS Center for Excellence in Quaternary Science and Global Change, Xi'an, 710061, China

[4]University of Chinese Academy of Sciences, Beijing, 100049, China

[*]Correspondence to: Guohui Li (ligh@ieecas.cn)

Abstract: Rapid increasing industries and city expansions have caused severe air pollution in the Guanzhong Basin (GZB), China in recent decades. Observations reveal that, although implementation of strict mitigation measures since 2014 has considerably reduced particulate matter (PM) pollution, the ozone (O_3) pollution during the warm season has continuously deteriorated in the basin. Simulations in May and August 2018 have been conducted using the WRF-Chem model to examine spatial and seasonal variations of the O_3 formation regimes as well as source attributions in the GZB. The model generally performs well in simulating meteorological parameters, O_3, NO_2, and fine PM against measurements. The identified O_3 formation regimes in cities of the GZB are all VOCs-sensitive in May and become more NO_X-sensitive in August. Sensitivity studies have shown that the power plants source generally suppresses the O_3 formation considerably in May and enhances it slightly in August due to its high NO_X and low VOCs emissions. The residential, transportation and industry sources increase the O_3 concentration in May and August. Moreover, the transportation and industry sources play an increasingly important role in August but opposite for the residential source. The variation of O_3 formation regimes and source attributions from May to August is caused by intensification of solar radiation, which not only promotes photochemical processes, also increases temperature and further enhances biogenic emissions

and vertical exchange in the planetary boundary layer. The present study can provide guidelines to devise the effective O_3 abatement strategies suitable for local situations.

Keywords: GZB, WRF-Chem model, O_3 formation regime, source attributions

1 Introduction

The issue of ozone (O_3) pollution has received considerable attention for the first time in the Los Angeles smog event in 1950s. Since then, the photochemical action of nitrogen oxides (NO_X) oxidizing hydrocarbons and thereby forming O_3 as well as concomitant photochemical oxidants has been discussed [*Haagen-Smit*, 1952]. Since 1990s, stringent precursor emission control strategies have been formulated and carried out to alleviate the severe O_3 pollution in many European and United States urban areas [*Cooper et al.*, 2012; *Cooper et al.*, 2015; *Derwent et al.*, 2010; *Simon et al.*, 2014]. Rapid industrialization and urbanization have caused severe air pollution in China within recent decades. The Chinese government has carried out aggressive emission mitigation measures since 2013 and considerably reduced particulate pollution, but widespread and persistent O_3 pollution frequently occurs in eastern China during the warm season from April to September. Observations from the Chinese monitoring network, the Ozone Monitoring Instrument, and the recent Tropospheric Ozone Assessment Report (TOAR) have all shown increasing near surface O_3 concentrations ($[O_3]$) and high occurrence frequency of severe O_3 pollution events in China [*G Li et al.*, 2017; *K Li et al.*, 2019a; *Lu et al.*, 2018; *Lu et al.*, 2019; *Shen et al.*, 2019].

O_3 is a typical secondary air pollutant produced in the troposphere by the photochemical oxidation of hydrocarbons and other volatile organic compounds (VOC_S) in the presence of NO_X and sunlight [*W Chameides and Walker*, 1973; *W L Chameides et al.*, 1992; *Fishman and Crutzen*, 1977; *Seinfeld*, 1989]. The intrusion from the stratosphere is also a critical dynamical source of the tropospheric O_3 [*Fishman and Crutzen*, 1978; *Junge*, 1962; *Mahlman et al.*, 1980; *Stohl*, 2003]. High $[O_3]$ can cause intractable hazards to the health of human, crops and ecosystems [*Lin et al.*, 2018; *Lippmann*, 1993; *Mauzerall et al.*, 2005], such as respiratory problems, aggravation asthma and reductions of the crop yields.

Furthermore, these adverse impacts of tropospheric O_3 are spatially and seasonally varied due to regionally different O_3 pollutions [*Daum*, 2004; *Y Wang et al.*, 2011]. Therefore, effective O_3 and precursors control strategies need to be designed for particular regions through identifying O_3 contributions from various emission sources, which is also called ozone source attributions.

Previous studies about O_3 source attributions are generally performed using chemical transport models incorporated with methodologies such as the brute force method (BFM), the decoupled direct method (DDM) and the ozone source apportionment technology (OSAT) with tagged tracers [*Dunker et al.*, 2002; *Napelenok et al.*, 2008; *Yarwood et al.*, 1996]. These source attribution approaches are widely used to evaluate O_3 contributions of its precursors from each emission sector or a specific region in China [*M Y Wang et al.*, 2019]. Studies on the O_3 source attribution provide fundamental understanding of the chemical and physical processes of O_3 formation, and offer sector or regional source targeted suggestions on O_3 pollution abatement. However, the photochemical regime of the O_3 formation in specific locations needs to be further examined to warrant effectiveness of the control strategies. The O_3 formation is traditionally classified in two chemical regimes, i.e., NO_X-limited or VOCs-limited. And the transition regime occurs when the O_3 formation is both sensitive to NO_X and VOCs emissions. Several methods have been used to identify the O_3 formation regime including chemistry-sensitive method like the Empirical Kinetic Modeling Approach (EKMA) [*Seinfeld*, 1988] and species indicators like O_3/NO_Z, H_2O_2/HNO_3 and $HCHO/NO_2$ [*L Li et al.*, 2011c; *Martin et al.*, 2004; *Sillman*, 1995].

Recent advances in O_3 source attributions in China have concentrated in the Beijing-Tianjin-Hebei (BTH) region [*G Li et al.*, 2017; *Liu et al.*, 2019], the Yangtze River Delta (YRD) region [*Gao et al.*, 2016; *L Li et al.*, 2019b] and the Pearl River Delta (PRD) region [*Y Li et al.*, 2013]. However, few studies have been conducted to investigate O_3 source

attributions in the Guanzhong Basin (GZB), which has suffered increasing O_3 pollution recently [*Feng et al.*, 2016]. The GZB, housing five cities in various development phase of urbanization and industrilization, is nestled between Qinling in the south and Loess Plateau in the north. The unique topography is unfavorable for the dispersion of air pollutants [*Bei et al.*, 2016a; *Bei et al.*, 2016b]. *Feng et al.* [2016] have found that the industrial emission sector is the largest contributor to [O_3] in Xi'an (the central city in the GZB) compared to biogenic and other anthropogenic sources in the summer of 2013. *N Li et al.* [2018] have disentangled the pure and synergistic effects of anthropogenic and/or biogenic sources on the O_3 formation in the GZB and revealed that the anthropogenic source alone dominates the O_3 formation.

Therefore, in the study, the WRF-Chem model is used to comprehensively investigate the O_3 source attributions and formation regime in the GZB during the warm seasons to support design and implementation of effective emission mitigation strategies for the O_3 pollution. The WRF-Chem model and observation data are described in Section 2. Model results and sensitivity studies are presented in Section 3, and the Conclusions are given in Section 4.

2 Data and method

2.1 WRF-Chem model and configurations

The WRF-Chem model (Weather Research and Forecasting model with Chemistry) [*Grell et al.*, 2005] utilized in this study is a specific version modified by *G Li et al* [2011a; 2012; 2010; 2011b]. Briefly, the SAPRC-99 mechanism (Statewide Air Pollution Research Centre, version 1999) is applied to simulate gas-phase chemistry, and the Community Multi-scale Air Quality (CMAQ) aerosol module (AERO5) developed by the US EPA is employed for the aerosol simulation [*Binkowski and Roselle*, 2003]. The Fast Tropospheric Ultraviolet and Visible (FTUV) radiation module with the aerosol and cloud effects on

112 photochemistry is incorporated into the model to calculate the photolysis rates of gas-phase
113 species [*G Li et al.*, 2005; *Tie et al.*, 2003]. The wet deposition of chemical species is based
114 on the method in the CMAQ module, and surface dry depositions are parameterized
115 according to *Wesely* [1989]. The inorganic components in the model are simulated using the
116 ISORROPIA Version 1.7 [*Nenes et al.*, 1998]. The secondary organic aerosol (SOA) is
117 predicted by a non-traditional SOA module, including the volatility basis set (VBS) modeling
118 approach and contributions from glyoxal and methylglyoxal [*G Li et al.*, 2011b].

119 Since O_3 pollution generally occurs during the warm season from April to September [*G*
120 *Li et al.*, 2017], May and August in the year of 2018, representing spring and summer
121 respectively, are selected for O_3 simulations in the GZB in the present study. Two days, 16th
122 May and 7th August, with the average peak 8-h [O_3] of 190 μg m^{-3} and 168 μg m^{-3}
123 respectively, are chosen for developing EKMA diagrams to examine the O_3 formation regime
124 in different areas. Figure 1 shows the model simulation domain and the detailed model
125 configuration can be found in Table 1.

126 The anthropogenic emission inventory is developed by *Zhang et al.* [2009] and the
127 biogenic emissions are calculated online using the Model of Emissions of Gases and Aerosols
128 from Nature (MEGAN) [*Guenther et al.*, 2006]. Figure 2 exhibits the distributions of
129 anthropogenic NO_X, VOCs and biogenic VOCs emission rates in May and August 2018.
130 High emissions of NO_X and anthropogenic VOCs (AVOCs) are concentrated at urban areas
131 of cities in the GZB, while the Qingling mountains, located in the south of the GZB, have
132 abundant biogenic VOCs emissions.

133 **2.2 Model sensitive studies**

134 An emission reduction matrix comprising 121 scenarios is designed to develop EKMA
135 diagrams to determine the O_3 formation regime. These scenarios include reductions of NO_X
136 and AVOCs emissions from 0% to 100% with an interval of 10%. Given that the biogenic

VOCs ($BVOC_S$) emissions are uncontrollable, only the AVOCs emission reduction is taken into consideration. Furthermore, the brute force method (BFM) is used to evaluate the O_3 contributions of industry, power, residential, transportation and biogenic sources in six cities in spring and summer. The BFM directly closes or cuts out one emission source to calculate its contribution to the O_3 formation[*Dunker et al.*, 1996]. Detailed description of simulation scenarios is shown in Table 2.

The O_3 formation is investigated in the five cities of the GZB, including Xi'an, Xianyang, Baoji, Weinan and Tongchuan (Figure 1b). The five cities are now experiencing different development phases of urbanization and industrialization. Xi'an, the provincial capital of Shaanxi, has been an industrialized city with the most population exceeding 10 million and the heavy traffic. In recent several years, with implementation of strict mitigation measures, industrial sectors with serious pollution have been decreased rapidly. Xianyang is now undergoing rapid industrialization and urbanization, followed by Baoji, Weinan, and Tongchuan. It is worth noting that Weinan is the city with the most power plants in the GZB. For comparison, the O_3 pollution in Hanzhong is also examined, a city located on the southern foot of Qinling Mountains and with less industrial activities and abundant forests surrounded (Figure 1).

2.3 Measurements

Measurements of criteria air pollutant concentrations and main meteorological parameters are used for evaluating the model performance. The hourly observations of $PM_{2.5}$, NO_2 and O_3 mass concentrations are released by the Ministry of Environment and Ecology of China. The meteorological parameters include the temperature and relative humidity at 2 m, wind speed and direction at 10 m at one site in the GZB (Figure 1b).

2.4 Statistical methods for model evaluation

For validation of the model performance, we follow performance guidelines for urban scale ozone modeling from the US EPA [*Doll*, 1991; *EPA*, 2005] and for aerosol modeling suggested by *Boylan and Russell* [2006]. Statistical methods for gas pollutants evaluation include the normalized mean bias (NMB) and the normalized mean error (NME), while the mean fractional bias (MFB) and mean fraction error (MFE) are recommended for aerosols validation. The basic statistical cores provided by the US EPA are also used for the evaluation, including the mean bias (MB) and the correlation coefficient (R).

$$NMB = \frac{\sum_{i=1}^{N}(P_i - O_i)}{\sum_{i=1}^{N} O_i} \times 100\%$$

$$NME = \frac{\sum_{i=1}^{N}|P_i - O_i|}{\sum_{i=1}^{N} O_i} \times 100\%$$

$$MFB = \frac{1}{N}\sum_{i=1}^{N}\frac{P_i - O_i}{O_i + P_i/2}$$

$$MFE = \frac{1}{N}\sum_{i=1}^{N}\frac{|P_i - O_i|}{O_i + P_i/2}$$

$$MB = \frac{1}{N}\sum_{i=1}^{N}(P_i - O_i)$$

$$R = \frac{\sum_{i=1}^{N}[(P_i - \bar{P}) \times (O_i - \bar{O})]}{\sqrt{\sum_{i=1}^{N}(P_i - \bar{P})^2 \times \sum_{i=1}^{N}(O_i - \bar{O})^2}}$$

Where P_i and O_i denote the predicted and observed variables, respectively. N is the total number of the predictions used for comparisons, and $\bar{P}$ and $\bar{O}$ denotes the average of the prediction and observation, respectively.

The model performance criteria suggested by the US EPA for O_3 regulatory applications are ±15% for NMB and below 30% for NME, and both MFB and MFE are less than or equal to approximately ±60% and +75%, respectively, for aerosols. For *MB*, the value of zero indicates that model underestimations and overestimations exactly cancel each other. The *R*

of 0 implies that there is no linear relationship; while the *R* of 1 means a perfect linear between the observations and simulations.

3 Results and discussions

3.1 O_3 pollutions in the GZB

To reduce $PM_{2.5}$ concentrations by up to 25% by 2017 compared with 2012 levels, the Chinese State Council has carried out the 'Air Pollution Prevention and Control Action Plan' (APPCAP) since September 2013. Implementation of the APPCAP has considerably reduced particulate pollution in China [*Zhang et al.*, 2019]. Table 3 provides the observed criteria air pollutant concentrations averaged from April to September in 2014 and 2018 in the GZB. CO, SO_2, $PM_{2.5}$ and PM_{10} concentrations have remarkably decreased, particularly regarding SO_2, with a reduction of 38% from 2014 to 2018. However, the average NO_2 and peak 8-h [O_3] have enhanced by 7.8% and 40.6%, respectively, showing that the O_3 pollution has continuously deteriorated in the GZB from 2014 to 2018 (Figure 3a).

O_3 observations from 5 cities with 33 ambient monitoring sites in the GZB as well as 4 sites in Hanzhong are analyzed to demonstrate the O_3 pollution condition in 2018. The O_3 pollution in the GZB generally occurs from April to August, with average peak 8-h [O_3] exceeding 100 μg m^{-3} (Figure 3b). Generally, maximum 8-h peak [O_3] emerge in June, while the average monthly [O_3] are the highest in August, attaining about 100 μg m^{-3}. The average peak 1-h [O_3] are all more than 130 μg m^{-3} in cities of the GZB and much higher in Xi'an and Xianyang than the other cities (Figure 4a). Furthermore, the observed maximum peak 1-h [O_3] are much higher in the GZB and Hanzhong, exceeding 200 μg m^{-3} (Figure 4b). Figure 4c and 4d display the days with the peak 1-h [O_3] exceeding 160 μg m^{-3} and 200 μg m^{-3} from April to August 2018, respectively. Four cities in the GZB have more than 60 (40%) days

with the peak 1-h [O_3] exceeding 160 μg m^{-3} and more than 15 (10%) days with the peak 1-h [O_3] exceeding 200 μg m^{-3}. Apparently, the O_3 pollution in the GZB are more serious and persistent compared with surrounding areas, and Xianyang is the most polluted city in the GZB, with the maximum peak 1-h [O_3] exceeding 300 μg m^{-3} and 45 (30%) days of the peak 1-h [O_3] more than 200 μg m^{-3} in the warm season of 2018.

3.2 Model performance

Considering the key role of meteorological conditions in air pollution simulations, Figures 5 and 6 show diurnal profiles of the simulated and observed near-surface temperature, relative humidity, wind speed and direction at Xianyang meteorological site in May and August, respectively. The WRF-Chem model reproduces successfully the temporal variations of the temperature in the two months, with the R exceeding 0.85, but overestimates the temperature against observations, with the MB ranging from 0.21 to 1.87 ^{o}C. The model also performs well in tracking the temporal variations of the near-surface RH, generally with the *R* more than 0.75. However, the model is subject to underestimating the RH, with the MB varying from -9.0% to -1.20%. The model reasonably simulates temporal variations of the near-surface wind speed compared to observations, with the R exceeding 0.5 and the MB less than 0.5 m s^{-1}, but fails to replicate the observed temporal variation of wind directions in August, with the R less than 0.36.

Figure 7 provides the predicted and observed horizontal distributions of average peak 8-h O_3 and NO_2 concentrations along with the simulated wind fields in May and August 2018 in the GZB. In the east of the GZB, the northeasterly wind is prevailing, causing transboundary transport of air pollutants from outside of the GZB. In the middle and west of the GZB, the wind is weak or disordered generally due to blocking of mountains, which is favorable for accumulation of air pollutants. The calculated near-surface 8-h O_3 and NO_2 distributions are generally consistent well with the observations at the ambient monitoring

sites. The average peak 8-h [O_3] in May exceed 100 μg m^{-3} in most areas of the GZB and the elevated NO_2 concentrations mainly occur in city areas, particularly in Xi'an (Figure 7a and 7b). In August, the average peak 8-h [O_3] increase to be more than140 μg m^{-3} in most areas of the GZB due to intensified solar radiation to enhance photochemical processes during daytime (Figure 7c and 7d).

Figure 8 depicts the temporal variations of simulated and observed near-surface O_3, NO_2 and $PM_{2.5}$ concentrations averaged over monitoring sites in the GZB in May and August 2018. The model overestimates O_3 and NO_2 concentrations slightly compared to observations in May (Figure 8a and 8b), with MBs of 9.2 μg m^{-3} and 1.6 μg m^{-3}, respectively. The NO_2 overestimations in19th to 22nd mainly result from model biases in simulating wind fields (Figure 5). O_3 and NO_2 concentrations in August are a little bit underestimated against observations, with MBs of -2.2 μg m^{-3} and -0.4 μg m^{-3}, respectively. The NMB and NME for simulated [O_3] range from -3 to 13% and from 19 to 28%, respectively, within the criteria from EPA guidelines (Table 4). The model also exhibits good performance in simulating $PM_{2.5}$ concentrations compared with observations, with the MFB of 0.1- 3.5% and MFE of 57-70%, which are within the model performance criteria suggested by *Boylan and Russell* [2006]. Table 4 shows the further validation of the WRF-Chem model simulations of O_3 and NO_2 in six cities, based on statistical methods suggested by previous studies [*EPA,* 2005]. The model generally performs reasonably in simulating O_3 and NO_2 in the six cities in May and August.

Generally, the simulated O_3, NO_2, and. $PM_{2.5}$ concentrations are generally in good agreement with observations, indicating that the WRF-Chem model is capable of representing major physical and chemical processes of tropospheric O_3 and well produces the temporal variations associated with synoptic conditions.

3.3 Spatial and seasonal variations of ozone formation regime

O_3 formation in the planetary boundary layer (PBL) is complicated, relying on its precursors of NO_X and VOCs from biogenic and various anthropogenic sources as well as solar radiation. Figures 9 and 10 provide the EKMA diagrams for the two O_3 pollution days in May and August in five cities of the GZB and Hanzhong. These diagrams are O_3 isopleths developed by reductions of NO_X and AVOCs emissions in sensitivity simulations. The NO_X-limited regime and VOCs-limited regime are separated by the ridge line, and areas closed to the line are defined as the transition regime, implying that the O_3 formation is in the same sensitivity to VOCs and NO_X emissions. The ridge line also indicates the maximum $[O_3]$ for given NO_X and AVOCs emissions to produce. The upper right of the corner is the start (base case) of the emission reduction scenarios with 100% AVOCs and 100% NO_X emissions. In the high O_3 pollution day in May, base scenarios of five cities in the GZB are all above ridge lines, showing that the O_3 formation is in a VOCs-limited regime. Further reduction in NO_X emissions or increase in VOCs emissions causes deterioration of the O_3 pollution. The base scenario of Hanzhong is closed to or on the ridge line, so the O_3 photochemical production is in the transition regime. Changes of the ratio of NO_X to VOCs emissions could increase or decrease $[O_3]$ in this regime. In August, the O_3 formation in Weinan and Baoji are still in a VOCs-limited regime, but it is in the transition regime in Xi'an and Xianyang, and becomes NOx-sensitive in Tongchuan. There is no ridge line in August in Hanzhong, as the O_3 formation is always NO_X-limited for any possible AVOCs-NO_X emission combinations.

The spatial variations of the O_3 formation regime can be attributed to the inhomogeneous distributions of O_3 precursors. As illustrated in Figure 2, high AVOCs emissions and BVOCs emissions mainly distribute in cities of the GZB and Qingling mountains, respectively. Given that the key species of VOCs emitted by plants and vegetables, such as isoprene and monoterpenes, are more chemically reactive than the main

AVOCs species, BVOCs are more effective to produce O_3 than AVOCs when they are of the same emission intensity and in NO_X-saturated conditions. There is a large amount of NO_X and AVOCs emission in cities of the GZB, but less BVOCs emissions. However, compared to cites in the GZB, Hanzhong is surrounded by abundant forests, and frequently influenced by high BVOCs emissions. Additionally, less industrial activities also lead to low NO_X and AVOCs emissions in the city. Therefore, this emission pattern of precursors causes the O_3 formation in Hanzhong to be more sensitive to NO_X than in cities of the GZB. The variation of the O_3 formation in cities of the GZB is attributed the different ratio of VOCs to NOx emissions.

The seasonal variations of the O_3 formation regime can be attributed to the changes in precursor emissions and solar radiation. AVOCs and NOx emissions in May (Figure 2a and 2b) and August (Figure 2d and 2e) are almost the same. The NOx and AVOCs emissions are increased by 1.2% and 1.6% from May to August in the GZB, which cannot explain the variation of the O_3 formation regime, i.e., the O_3 production in all six cities tends to be more NO_X-sensitive in August than May (Figure 10). The most important change from May to August is the intensification of solar radiation and the resultant increase in air temperature. Firstly, BVOCs emissions are dependent on solar radiation and air temperature, so increased solar radiation and air temperature in August enhance BVOCs emissions, providing more background VOCs for O_3 formation and shifting the O_3 formation regime to be more NOx-sensitive. Secondly, enhancement of solar radiation and higher temperature in August facilitate photochemical reactions and escalate atmospheric oxidation capability. Higher temperature is also favorable for development of the planetary boundary layer and vertical exchange of air pollutants in the PBL, decreasing concentrations of near-surface O_3 precursors. Increase in HOx radicals due to active photochemical processes causes the HO_X-loss to be dominated by self-reaction of peroxy radicals rather than reactions of NO_2

with OH, further shifting O_3 production to be more NO_X-sensitive (Figure 11). This seasonal transition trend is also found in several previous studies. For examples, *Wu and Xie* [2017] have discussed occurrence of a switch from a NO_X-saturated to NO_X-sensitive O_3 formation regime in most suburban and rural areas in China when summer arrives. *Ou et al.* [2016] have proposed that O_3 formation shifts toward VOC-limited conditions in the PRD from summer to autumn. The O_3 formation regime in cities of the GZB varies from being NO_X-sensitive to VOCs-sensitive in August, showing different ratios of VOCs to NO_X emissions. Therefore, different emission mitigation strategies need to be devised and implemented for cities in the GZB to reduce the O_3 pollution.

3.4 Ozone source attributions

In this section, the peak 8-h O_3 contributions of industrial, residential, transportation, power plants and biogenic sources are evaluated in May and August using the BFM in five cities of the GZB and Hanzhong.

Figure 12 represents spatial distributions of average near-surface peak 8-h O_3 contributions of various anthropogenic and biogenic emissions in May. The biogenic source plays a more important role in the O_3 formation than the four anthropogenic sources, with the O_3 contribution of 5~20 μg m^{-3} in the GZB and Hanzhong, particularly in the middle and east of the GZB (including Xi'an, Weinan and Tongchuan) where the O_3 contribution exceeds 10 μg m^{-3}. The O_3 contribution of the industry source generally is about 5~20 μg m^{-3} in the GZB but is negative in the area with high industrial NO_X emissions causing titration of O_3. The residential and transportation sources play a considerable role in the O_3 formation, contributing about 5~10 μg m^{-3} O_3 generally, but the transportation source is subject to decreasing [O_3] in the city center. Apparently, the O_3 formations around the power plants are significantly suppressed by the high NO_X emission, decreasing [O_3] by up to 30 μg m^{-3}. The power source also decreases [O_3] in the middle and east of the GZB by more than 5 μg m^{-3}.

330 The adverse contribution of biogenic and power plants sources on the O_3 formation in the
331 middle and east of the GZB can be explained by the chemical regime. The O_3 production of
332 those areas in May is generally in the VOCs-sensitive regime (as Figure 9 shows), so the
333 biogenic emissions (mainly BVOCs) increase [O_3] while the power plants emissions (mainly
334 NO_X) play an opposite role.

335 The horizontal distributions of average peak 8-h O_3 contributions of biogenic and
336 various anthropogenic sources in August are provided in Figure 13. Biogenic and industry
337 sources play a more important role in the O_3 formation than the other sources, contributing
338 20~50 μg m^{-3} O_3 in the middle of the GZB (including Xi'an and Xianyang) and 5~30 μg m^{-3}
339 O_3 in Hanzhong, respectively. Different from the O_3 contribution in May, the transportation
340 source consistently increases the [O_3] by 10~30 μg m^{-3} in the GZB and 10~20 μg m^{-3} in
341 Hanzhong. The power plants source in August only suppresses the O_3 production around the
342 source locations but enhances the O_3 formation by 5~20 μg m^{-3} in the rest area of the GZB.
343 The O_3 contribution of the residential source is not significant when comparing to the other
344 sources, ranging from 5 to 20 μg m^{-3} in the GZB. Since the O_3 formation regime becomes
345 more NO_X-sensitive in August than in May, the sources with high NO_X emissions, such as
346 industry, power plants and transportation, play an increasingly important role in the O_3
347 formation.

348 Figure 14 exhibits the average peak 8-h O_3 contributions of industry, transportation,
349 power plants, residential and biogenic sources in cities of GZB in May and August. In May,
350 the power plants emissions are the main sources to suppress the O_3 formation in all cities
351 except Hanzhong due to its transition O_3 formation regime. All emission sources promote the
352 O_3 production in the six cities in August except the power plants in Weinan (Figure 14b),
353 which can be attributed to the VOCs-sensitive O_3 formation regime. The biogenic source
354 plays the most important role in the O_3 pollution in May in the six cities, whereas industry,

biogenic and transportation sources become chief contributors to increase [O_3] in August. It is worth noting that the power plants source significantly lowers [O_3] in Weinan whether in May or August due to its massive NO_X emissions.

Table 5 provides the O_3 contribution of various sources in the six cities. The O_3 contribution of the power plants source manifests considerable seasonal differences while the residential source does not show significant seasonal variations. The power pants source plays an opposite role in the O_3 production in May and August in cities of the GZB. For example, the source decreases [O_3] by about 7.3% in Xi'an and 5.9% in Xianyang in May while increases [O_3] by 4.0% in Xi'an and 7.0% in Xianyang in August. The transportation source enhances [O_3] by 3.9~13.9% in August in the six cities, but only contributes 2.2~6% of [O_3] in May. Same as the transportation source, the industry and biogenic sources are more effective in enhancing O_3 formation in August than in May. These seasonal differences of source contributions can be chiefly attributed to the variations of the O_3 formation regime analyzed in Section 3.3.

4 Summary and conclusions

Observations have shown that the O_3 pollution, generally occurring from April to August, has continuously deteriorated in the GZB since 2014. Simulations in May and August 2018 have been performed using the WRF-Chem model to investigate the O_3 source attributions and formation regime for design and implementation of effective emission mitigation strategies to alleviate the worsening O_3 pollution in the GZB. The model generally performs reasonably well in simulating the meteorological parameters, O_3, NO_2, and $PM_{2.5}$ against observations in the GZB.

Two O_3 pollution days in May and August 2018 are selected to develop the EKMA diagrams by reductions of NO_X and AVOCs emissions in sensitivity simulations for five

cities in the GZB and Hanzhong with less industrial activities and more influence of biogenic emissions. Results show that the O_3 formation in May is VOCs-sensitive in five cities of the GZB but in the transition regime in Hanzhong. However, in August with intensification of solar radiation, the O_3 formation regime in cities of the GZB and Hanzhong becomes more NO_X-sensitive. The O_3 formation is still VOCs-sensitive in Baoji and Weinan, shifts to the transition regime in Xi'an and Xianyang, and becomes NO_X-sensitive in Tongchuan and Hanzhong.

The BFM is utilized to estimate the O_3 contributions of various anthropogenic and biogenic sources. The biogenic source plays the most important role in the O_3 formation in May, with the O_3 contribution ranging from 9% to 15% in the six cities. The power plant source suppresses the O_3 formation in cities of the GZB, decreasing the [O_3] by more than 40% in Weinan, but slightly increase [O_3] in Hanzhong due to influence of biogenic emissions. The residential, transportation and industry sources increase the [O_3] in cities of the GZB by 2~8%. In August, the O_3 contribution of the biogenic source is still important, ranging from 10% to 20%. Except in Weinan, the power plant source also increases [O_3] by 2~8%. The O_3 contribution of the industry source varies from 6% to 17% in the six cities, exceeding the biogenic source in Xianyang. In addition, the transportation source also plays a considerable role in the O_3 formation, but the O_3 contribution of the residential source is not significant, less than 5%. The variation of O_3 formation regimes and source attributions from May to August can be interpreted by intensification of solar radiation, which not only promote photochemical processes, also increases temperature and further enhances biogenic emissions and vertical exchange in the PBL.

The spatial and seasonal characteristics of O_3 formation regimes and source attributions in the GZB presented in the study can provide insights into the governing processes controlling the O_3 pollution formation and guidelines to devise the effective O_3 abatement

strategies suitable for local situations. For example, in May, reducing AVOCs emissions is optimum in cities of the GZB, but emphases need to be put on different sources for the five cities. For example, emissions of the residential need to be controlled for the O_3 pollution in Xi'an but industrial emissions are proposed to be curbed Xianyang in May. However, in August, unified emission control measures, i.e., reducing AVOCs or NO_X emissions, cannot be devised because of different O_3 formation regimes in cities of the GZB. The AVOCs emissions need to be controlled still in Weinan and Baoji due to the VOCs-limited regime, but in Tongchuan, mitigation of NO_X emissions become necessary due to the NO_X-limited regime. In Xi'an and Xianyang, the design of anthropogenic emission mitigation is delicate since the O_3 formation is in the transition regime and might be both sensitive to NO_X and VOCs emissions.

Generally, the WRF-Chem model performs well in simulating the O_3 pollution in the GZB, but model biases still exist, which might be caused by uncertainties in simulations of meteorological fields and the emission inventory. It is worth noting that the emission inventory has undergone rapid changes since implementation of strict mitigation measures in 2014 in the GZB. Future works need to be conducted based on the improved meteorological field simulations and the updated emission inventory.

Acknowledgments. We would like to acknowledge the National Oceanic and Atmospheric Administration (NOAA) for ambient weather station observations which are freely obtained from the website http://gis.ncdc.noaa.gov/maps. The hourly ambient surface O_3, NO_2 and $PM_{2.5}$ mass concentrations are real-timely released by Ministry of Environmental Protection, China on the website http://www.aqistudy.cn/, freely downloaded from

http://106.37.208.233:20035/. This work is financially supported by the National Key R&D Plan (Quantitative Relationship and Regulation Principle between Regional Oxidation Capacity of Atmospheric and Air Quality (2017YFC0210000)) and National Research Program for Key Issues in Air Pollution Control (DQGG0105).

Reference

Bei, N., G. Li, R. Huang, J. Cao, N. Meng, T. Feng, S. C. Liu, T. Zhang, Q. Zhang, and L. T. Molina (2016a), Typical synoptic situations and their impacts on the wintertime air pollution in the Guanzhong basin, China, *Atmos. Chem. Phys.*, *11*, 7373-7387, doi:10.5194/acp-16-7373-2016.

Bei, N., B. Xiao, N. Meng, and T. Feng (2016b), Critical role of meteorological conditions in a persistent haze episode in the Guanzhong basin, China, *Sci. Total Environ.*, *550*, 273-284, doi:10.1016/j.scitotenv.2015.12.159.

Binkowski, F. S., and S. J. Roselle (2003), Models-3 Community Multiscale Air Quality (CMAQ) model aerosol component 1. Model description, *J. Geophys. Res. Atmos.*, *108*(D6), doi:10.1029/2001jd001409.

Boylan, J. W., and A. G. Russell (2006), PM and light extinction model performance metrics, goals, and criteria for three-dimensional air quality models, *Atmos. Environ.*, *40*(26), 4946-4959, doi:10.1016/j.atmosenv.2005.09.087.

Chameides, W., and J. C. G. Walker (1973), A photochemical theory of tropospheric ozone, *J. Geophys. Res.*, *78*(36), 8751-8760, doi:10.1029/JC078i036p08751.

Chameides, W. L., et al. (1992), Ozone Precursor Relationships in the Ambient Atmosphere, *J. Geophys. Res.*, *97*, 6037-6055.

Cooper, O. R., R.-S. Gao, D. Tarasick, T. Leblanc, and C. Sweeney (2012), Long-term ozone trends at rural ozone monitoring sites across the United States, 1990-2010, *J. Geophys. Res. Atmos.*, *117*(D22), n/a-n/a, doi:10.1029/2012jd018261.

Cooper, O. R., A. O. Langford, D. D. Parrish, and D. W. Fahey (2015), Challenges of a lowered U.S. ozone standard.pdf, *Science*, *348*(6239), 1096-1097.

Daum, P. H. (2004), Origin and properties of plumes of high ozone observed during the Texas 2000 Air Quality Study (TexAQS 2000), *J. Geophys. Res.*, *109*(D17), doi:10.1029/2003jd004311.

Derwent, R. G., C. S. Witham, S. R. Utembe, M. E. Jenkin, and N. R. Passant (2010), Ozone in Central England: the impact of 20 years of precursor emission controls in Europe, *Environ. Sci. Policy*, *13*(3), 195-204, doi:10.1016/j.envsci.2010.02.001.

Doll, D. (1991), Guideline for regulatory application of the Urban Airshed Model*Rep.*, Environmental Protection Agency, Research Triangle Park, NC (United States)

Dunker, A. M., R. E. Morris, A. K. Pollack, C. H. Schleyer, and G. Yarwood (1996), Photochemical modeling of the impact of fuels and vehicles on urban ozone using auto/oil program data, *Environ. Sci. Technol.*, *30*(3), 787-801.

Dunker, A. M., G. Yarwood, J. P. Ortmann, and G. M. Wilson (2002), Comparison of Source Apportionment and Source Sensitivity of Ozone in a Three-Dimensional Air Quality Model, *Environ. Sci. Technol.*, *36*, 2953-2964.

EPA, U. (2005), Guidance on the Use of Models and Other Analyses in Attainment Demonstrations for the 8-hour Ozone NAAQS*Rep.*, EPA-454/R-05-002.

Feng, T., et al. (2016), Summertime ozone formation in Xi'an and surrounding areas, China, *Atmos. Chem. Phys.*, *7*, 4323-4342, doi:10.5194/acp-16-4323-2016.

Fishman, J., and P. J. Crutzen (1977), A numerical study of tropospheric photochemistry using a one-dimensional model, *J. Geophys. Res.*, *82*(37), 5897-5906, doi:10.1029/JC082i037p05897.

Fishman, J., and P. J. Crutzen (1978), The origin of ozone in the troposphere, *Nature*, *274*, 855-858.

Gao, J., B. Zhu, H. Xiao, H. Kang, X. Hou, and P. Shao (2016), A case study of surface ozone source apportionment during a high concentration episode, under frequent shifting wind conditions over the Yangtze River Delta, China, *Sci. Total Environ.*, *544*, 853-863, doi:10.1016/j.scitotenv.2015.12.039.

Grell, G. A., S. E. Peckham, R. Schmitz, S. A. McKeen, G. Frost, W. C. Skamarock, and B. Eder (2005), Fully coupled "online" chemistry within the WRF model, *Atmos. Environ.*, *39*(37), 6957-6975, doi:10.1016/j.atmosenv.2005.04.027.

Guenther, A., T. Karl, P. Harley, C. Wiedinmyer, P. I. Palmer, and C. Geron (2006), Estimates of global terrestrial isoprene emissions using MEGAN (Model of Emissions of Gases and Aerosols from Nature).pdf, *Atmos. Chem. Phys.*, *11*, 3181-3210.

Haagen-Smit, A. J. (1952), Chemistry and Physiology of Los Angeles Smog, *Ind. Eng. Chem. Res.*, *44*(6), 1342-1346, doi:10.1021/ie50510a045.

Junge, C. E. (1962), Global ozone budget and exchange between stratosphere and troposphere, *Tellus B*, *14*, 363-377.

Li, G., N. Bei, J. Cao, J. Wu, X. Long, T. Feng, W. Dai, S. Liu, Q. Zhang, and X. Tie (2017), Widespread and persistent ozone pollution in eastern China during the non-winter

season of 2015: observations and source attributions, *Atmos. Chem. Phys.*, *17*(4), 2759-2774, doi:10.5194/acp-17-2759-2017.

Li, G., N. Bei, X. Tie, and L. T. Molina (2011a), Aerosol effects on the photochemistry in Mexico City during MCMA-2006/MILAGRO campaign, *Atmos. Chem. Phys.*, *11*(11), 5169-5182, doi:10.5194/acp-11-5169-2011.

Li, G., W. Lei, N. Bei, and L. T. Molina (2012), Contribution of garbage burning to chloride and PM2.5 in Mexico City, *Atmos. Chem. Phys.*, *12*(18), 8751-8761, doi:10.5194/acp-12-8751-2012.

Li, G., W. Lei, M. Zavala, R. Volkamer, S. Dusanter, P. Stevens, and L. T. Molina (2010), Impacts of HONO sources on the photochemistry in Mexico City during the MCMA-2006/MILAGO Campaign, *Atmos. Chem. Phys.*, *10*(14), 6551-6567, doi:10.5194/acp-10-6551-2010.

Li, G., M. Zavala, W. Lei, A. P. Tsimpidi, V. A. Karydis, S. N. Pandis, M. R. Canagaratna, and L. T. Molina (2011b), Simulations of organic aerosol concentrations in Mexico City using the WRF-CHEM model during the MCMA-2006/MILAGRO campaign, *Atmos. Chem. Phys.*, *11*(8), 3789-3809, doi:10.5194/acp-11-3789-2011.

Li, G., R. Zhang, J. Fan, and X. Tie (2005), Impacts of black carbon aerosol on photolysis and ozone, *J. Geophys. Res.*, *110*(D23), doi:10.1029/2005jd005898.

Li, K., D. J. Jacob, H. Liao, L. Shen, Q. Zhang, and K. H. Bates (2019a), Anthropogenic drivers of 2013-2017 trends in summer surface ozone in China, *Proc. Natl. Acad. Sci. U. S. A.*, *116*(2), 422-427, doi:10.1073/pnas.1812168116.

Li, L., J. An, L. Huang, R. Yan, C. Huang, and G. Yarwood (2019b), Ozone source apportionment over the Yangtze River Delta region, China: Investigation of regional transport, sectoral contributions and seasonal differences, *Atmos. Environ.*, *202*, 269-280, doi:10.1016/j.atmosenv.2019.01.028.

Li, L., et al. (2011c), Ozone sensitivity analysis with the MM5-CMAQ modeling system for Shanghai, *J. Environ. Sci.*, *23*(7), 1150-1157, doi:10.1016/s1001-0742(10)60527-x.

Li, N., Q. He, J. Greenberg, A. Guenther, J. Li, J. Cao, J. Wang, H. Liao, Q. Wang, and Q. Zhang (2018), Impacts of biogenic and anthropogenic emissions on summertime ozone formation in the Guanzhong Basin, China, *Atmos. Chem. Phys.*, *18*(10), 7489-7507, doi:10.5194/acp-18-7489-2018.

Li, Y., A. K. H. Lau, J. C. H. Fung, H. Ma, and Y. Tse (2013), Systematic evaluation of ozone control policies using an Ozone Source Apportionment method, *Atmos. Environ.*, *76*, 136-146, doi:10.1016/j.atmosenv.2013.02.033.

Lin, Y., F. Jiang, J. Zhao, G. Zhu, X. He, X. Ma, S. Li, C. E. Sabel, and H. Wang (2018), Impacts of O3 on premature mortality and crop yield loss across China, *Atmos. Environ.*, *194*, 41-47, doi:10.1016/j.atmosenv.2018.09.024.

Lippmann, M. (1993), Use of human lung tissue for studies of structural changes associated with chronic ozone exposure: opportunities and critical issues, *Environ. Health Persp.*, *101*, 209-212.

Liu, H., M. Zhang, X. Han, J. Li, and L. Chen (2019), Episode analysis of regional contributions to tropospheric ozone in Beijing using a regional air quality model, *Atmos. Environ.*, *199*, 299-312, doi:10.1016/j.atmosenv.2018.11.044.

Lu, X., J. Hong, L. Zhang, O. R. Cooper, M. G. Schultz, X. Xu, T. Wang, M. Gao, Y. Zhao, and Y. Zhang (2018), Severe Surface Ozone Pollution in China: A Global Perspective, *Environ. Sci. Technol.*, *5*(8), 487-494, doi:10.1021/acs.estlett.8b00366.

Lu, X., L. Zhang, Y. Chen, M. Zhou, B. Zheng, K. Li, Y. Liu, J. Lin, T.-M. Fu, and Q. Zhang (2019), Exploring 2016–2017 surface ozone pollution over China: source contributions and meteorological influences, *Atmos. Chem. Phys.*, *19*(12), 8339-8361, doi:10.5194/acp-19-8339-2019.

Mahlman, J. D., H. Levy, and W. J. Moxim (1980), Three-Dimansional Tracer Structure and Behavior as Simulated in Two Ozone Precursor Experiments.pdf, *J. Atmos. Sci.*, *37*(3), 655-685.

Martin, R. V., A. M. Fiore, and A. Van Donkelaar (2004), Space-based diagnosis of surface ozone sensitivity to anthropogenic emissions, *Geophys. Res. Lett.*, *31*(6), n/a-n/a, doi:10.1029/2004gl019416.

Mauzerall, D., B. Sultan, N. Kim, and D. Bradford (2005), NO emissions from large point sources: variability in ozone production, resulting health damages and economic costs, *Atmos. Environ.*, *39*(16), 2851-2866, doi:10.1016/j.atmosenv.2004.12.041.

Napelenok, S. L., D. S. Cohan, M. T. Odman, and S. Tonse (2008), Extension and evaluation of sensitivity analysis capabilities in a photochemical model, *Environ. Modell. Softw.*, *23*(8), 994-999, doi:10.1016/j.envsoft.2007.11.004.

559 Nenes, A., S. N. Pandis, and C. Pilinis (1998), ISORROPIA: A new thermodynamic
560 equilibrium model for multiphase multicomponent inorganic aerosols.pdf, *Aquat.*
561 *Geochem.*, *4*, 123-152.

562 Ou, J., Z. Yuan, J. Zheng, Z. Huang, M. Shao, Z. Li, X. Huang, H. Guo, and P. K. Louie
563 (2016), Ambient Ozone Control in a Photochemically Active Region: Short-Term
564 Despiking or Long-Term Attainment?, *Environ. Sci. Technol.*, *50*(11), 5720-5728,
565 doi:10.1021/acs.est.6b00345.

566 Seinfeld, J. H. (1988), Ozone air quality models. A critical review, *JAPCA*, *38*(5), 616-645,
567 doi:10.1080/08940630.1988.10466404.

568 Seinfeld, J. H. (1989), Urban Air Pollution: State of the Science, *Science*, *243*, 745-752.

569 Shen, L., D. J. Jacob, X. Liu, G. Huang, K. Li, H. Liao, and T. Wang (2019), An evaluation
570 of the ability of the Ozone Monitoring Instrument (OMI) to observe boundary layer
571 ozone pollution across China: application to 2005–2017 ozone trends, *Atmos. Chem.*
572 *Phys.*, *19*(9), 6551-6560, doi:10.5194/acp-19-6551-2019.

573 Sillman, S. (1995), The use of NOy, H202, and HNO3 as indicators for
574 ozone-NOx-hydrocarbon sensitivity in urban locations, *J. Geophys. Res.*, *100*,
575 14,175-114,188.

576 Simon, H., A. Reff, B. Wells, J. Xing, and N. Frank (2014), Ozone trends across the United
577 States over a period of decreasing NOx and VOC emissions, *Environ. Sci. Technol.*,
578 *49*(1), 186-195, doi:10.1021/es504514z.

579 Stohl, A. (2003), Stratosphere-troposphere exchange: A review, and what we have learned
580 from STACCATO, *J. Geophys. Res.*, *108*(D12), doi:10.1029/2002jd002490.

581 Tie, X., S. Madronich, S. Walters, R. Zhang, P. Pasch, and W. Collins (2003), Effect of
582 clouds on photolysis and oxidants in the troposphere, *J. Geophys. Res.*, *108*(D20),
583 doi:10.1029/2003jd003659.

584 Wang, M. Y., S. H. L. Yim, D. C. Wong, and K. F. Ho (2019), Source contributions of
585 surface ozone in China using an adjoint sensitivity analysis, *Sci. Total Environ.*, *662*,
586 385-392, doi:10.1016/j.scitotenv.2019.01.116.

587 Wang, Y., Y. Zhang, J. Hao, and M. Luo (2011), Seasonal and spatial variability of surface
588 ozone over China: contributions from background and domestic pollution, *Atmos. Chem.*
589 *Phys.*, *11*(7), 3511-3525, doi:10.5194/acp-11-3511-2011.

590 Wesely, M. L. (1989), Parameterization of surface resistances to gaseous dry deposition in
591 regional-scale numerical models.pdf, *Atmos. Environ.*, *23*, 1293-1304.

592 Wu, R., and S. Xie (2017), Spatial Distribution of Ozone Formation in China Derived from
593 Emissions of Speciated Volatile Organic Compounds, *Environ. Sci. Technol.*, *51*(5),
594 2574-2583, doi:10.1021/acs.est.6b03634.

595 Yarwood, G., R. Morris, M. Yocke, H. Hogo, and T. Chico (1996), Development of a
596 methodology for source apportionment of ozone concentration estimates from a
597 photochemical grid model, *J. Air Waste Manage., Pittsburgh, PA 15222(USA).[np]*.

598 Zhang, Q., et al. (2009), Asian emissions in 2006 for the NASA INTEX-B mission.pdf,
599 *Atmos. Chem. and Phys.*, 5131-5153.

600 Zhang, Q., et al. (2019), Drivers of improved PM2.5 air quality in China from 2013 to 2017,
601 *Proc. Natl. Acad. Sci. U. S. A.*, *116*(49), 24463-24469, doi:10.1073/pnas.1907956116.

602

603

604

605

606 Table 1 WRF-Chem model configurations.

607

Region	**Guanzhong Basin (GZB)**
Simulation period	01-31 May and 02 Aug. to 01 Sep. 2018
Domain size	150×150
Domain center	34.25°N, 109°E
Horizontal resolution	6km × 6km
Vertical resolution	35 vertical levels with a stretched vertical grid with spacing ranging from 30m near the surface to 500m at 2.5 km and 1 km above 14 km
Microphysics scheme	WRF Single-Moment six-class graupel scheme (Hong and Lim, 2006)
Boundary layer scheme	Mellor–Yamada–Janjic turbulent kinetic energy scheme (Janjic, 2002)
Surface layer scheme	MYJ surface scheme (Janjic, 2002)
Land-surface scheme	Unified Noah land-surface model (Chen and Dudhia, 2001)
Longwave radiation scheme	Goddard longwave scheme (Chou and Suarez, 2001)
Shortwave radiation scheme	Goddard shortwave scheme (Chou and Suarez, 1999)
Meteorological boundary and initial conditions	NCEP 1°×1°reanalysis data
Chemical initial and boundary conditions	WACCM 6-h output
Anthropogenic emission inventory	SAPRC-99 chemical mechanism emissions (Zhang et al., 2009)
Biogenic emission inventory	MEGAN model developed by Guenther et al. (2006)

608

609

610

611 Table 2 Description of simulation scenarios for O_3 attributions.

612

Case	Emissions input
f_{all}	With all anthropogenic and biogenic emissions
f_{ind}	Without industry emissions
f_{tra}	Without transportation emissions
f_{pow}	Without power plant emissions
f_{res}	Without residential emissions
f_{bio}	Without biogenic emissions

613 f_{all}: the base case; $f_{all} - f_{ind}$: the contribution of industry emissions; $f_{all} - f_{tra}$: the contribution of transportation
614 emissions; $f_{all} - f_{pow}$: the contribution of power plants emissions; $f_{all} - f_{res}$: the contribution of residential emissions;
615 $f_{all} - f_{bio}$: the contribution of biogenic emissions.

616

617

618

Table 3 Observed hourly mass concentrations of pollutants averaged from April to August in 2014 and 2018 in the Guanzhong Basin.

Pollutants	**CO (mg m^{-3})**	**SO_2 (μg m^{-3})**	**NO_2 (μg m^{-3})**	**O_3 (μg m^{-3})**	**$PM_{2.5}$ (μg m^{-3})**	**PM_{10} (μg m^{-3})**
2014	1.21	14.9	33.3	90.9	46.3	105.2
2018	0.88	9.2	35.9	127.8	35.8	89.8
Change (%)	-27.3	-38.3	+7.8	+40.6	-22.7	-14.6

CO, SO_2, NO_2, $PM_{2.5}$ and PM_{10} are hourly average concentrations. O_3 are average concentrations from 11:00 to 18:00 BJT.

626 Table 4 Validation of WRF-Chem model performance on simulations of air pollutants in six cities.

627

Cities	Species	May			August		
		MB ($\mu g\ m^{-3}$)	NMB	NME	MB ($\mu g\ m^{-3}$)	NMB	NME
XA	O_3	9.3	12.7%	29.0%	-3.6	-3.5%	24.9%
	NO_2	3.1	6.1%	25.4%	-1.4	-3.9%	22.9%
XY	O_3	7,1	11.4%	29.1%	-9.1	-7.5%	23.6%
	NO_2	1.6	3.4%	26.7%	1.5	5.5%	28.8%
BJ	O_3	10.4	14.2%	29.5%	7.6	8.8%	25.8%
	NO_2	1.2	3.4%	25.9%	0.3	1.3%	27.2%
WN	O_3	9,5	13.1%	29.1%	-9.2	-7.6%	23.8%
	NO_2	1.1	2.4%	28.7%	1.3	5.0%	26.8%
TC	O_3	4.0	4.4%	28.8%	-3.0	-3.1%	24.6%
	NO_2	-1.0	-3.5%	23.8%	-0.5	-2.5%	28.0%
HZ	O_3	1.5	2.0%	28.4%	7.4	9.0%	26.6%
	NO_2	-0.0	-0.2%	24.7%	0.5	3.4%	25.7%

628 XA, XY, WN, BJ, TC and HZ represent the city of Xi'an, Xianyang, Weinan, Baoji, Tongchuan and Hanzhong respectively.

629 Ref. criteria: within ±15% for NMB and below 30% for NME (EPA, 2005).

630

631

632

633 Table 5 O_3 contribution of various sources in the six cities in May and August.

634

Seasons	Cities	Peak 8-h O_3 contribution					
		Anthro	Ind	Tra	Pow	Res	Bio
Spring (May)	XA	25.8%	3.9%	2.2%	-7.3%	7.3%	10.0%
	XY	31.3%	7.1%	3.9%	-5.9%	6.5%	10.7%
	BJ	24.5%	3.5%	5.2%	-3.2%	4.9%	9.2%
	WN	-2.3%	6.4%	4.8%	-41.6%	3.4%	14.4%
	TC	28.8%	5.8%	4.2%	-1.3%	3.5%	10.4%
	HZ	18.8%	-3.4%	6.0%	1.7%	0.7%	9.5%
Summer (August)	XA	47.2%	14.6%	8.8%	4.0%	4.9%	15.8%
	XY	52.0%	16.8%	10.8%	7.0%	4.7%	15.3%
	BJ	46.1%	14.2%	9.2%	3.7%	3.1%	10.8%
	WN	17.2%	9.7%	3.9%	-28.5%	1.5%	20.5%
	TC	40.2%	7.1%	6.8%	8.2%	2.0%	15.1%
	HZ	32.5%	6.6%	13.9%	2.3%	1.5%	18.3%

635 XA, XY, WN, BJ, TC and HZ represent the urban areas in Xi'an, Xianyang, Weinan, Baoji, Tongchuan and Hanzhong
636 respectively. Anthro, Ind, Tra, Pow, Res, and Bio represent total anthropogenic, industry, transportation, power plants,
637 residential, and biogenic source, respectively.

638

639

640

Figure Captions

Figure 1 WRF-Chem simulation domain with topography. The filled black circles represent centers of cities with ambient monitoring sites and the size of circles denotes the number of ambient monitoring sites of cities. The diamond denotes the meteorological observation station. The areas surrounded by deep blue lines are focused in this study (GZB and Hanzhong city).

Figure 2 Spatial distribution of (a)/(d) anthropogenic NO_X, (b)/(e) anthropogenic VOCs, and (c)/(f) biogenic isoprene emission rates in May/August.

Figure 3 (a) trends of observed average peak 8-h [O_3] in warm seasons (from April to August) in the GZB from 2014 to 2018, and (b) maximum peak 8-h [O_3] (dark blue line), average peak 8-h daily [O_3] (light blue line) and monthly average [O_3] (yellow line) in 2018 in the GZB. The red line indicates the first grade of National Ambient Air Quality Standards for average peak 8-h daily [O_3] in China.

Figure 4 Distribution of observed (a) average daily peak 1-h [O_3], (b) maximum daily peak 1-h [O_3], (c) days with the observed peak 1h [O_3] exceeding 160 μg m^{-3} and (d) days with the observed peak 1-h [O_3] exceeding 200 μg m^{-3} in the GZB and surrounding areas from April to August 2018.

Figure 5 Temporal variations of predicted (red) and observed (black) (a) temperature at 2 m, (b) relative humid at 2 m, (c) wind direction and (d) wind speed at 10 m at Xianyang meteorological monitoring site in May 2018. The model performance statistic metrics of MB and R are also shown.

Figure 6 Same as Figure 5, but for August 2018.

Figure 7 Pattern comparisons of simulated versus observed average (a)/(c) daily peak 8-h O_3 and (b)/(d) NO_2 concentrations in May/August 2018. Colored circles: O_3 observations; color contour: O_3 simulations; black arrows: simulated near-surface winds.

Figure 8 Diurnal profiles of measured (black dots) and predicted (red line) (a)/(d) O_3, (b)/(e) NO_2 and (c)/(f) $PM_{2.5}$ concentrations averaged over all ambient monitoring stations in the GZB in May/August 2018.

Figure 9 O_3 isopleth profiles (μg m^{-3} of average daily peak 8-h concentrations) in urban areas of (a) Xi'an, (b) Xianyang, (c) Weinan, (d) Baoji, (e) Tongchuan and (f) Hanzhong on16 May 2018. The VOC-limited and NOx-limited regimes are separated by the red ridge lines.

Figure 10 Same as Figure 9, but for 7 August 2018.

Figure 11 Average daytime NO_2, HO_2 and HO concentrations during springtime on 16 May 2018 and 7 August 2018 in urban areas of (a) Xi'an, (b) Xianyang, (c) Weinan, (d) Baoji, (e) Tongchuan and (f) Hanzhong.

Figure 12 Distributions of the average peak 8-h O_3 contribution in May 2018 from (a) industry, (b) transportation, (c) residential, (d) power plants, (e) total anthropogenic, and (f) biogenic sources.

Figure 13 Same as Figure 12, but for August 2018.

Figure 14 Average peak 8-h O_3 contributions from various sources in (a) May and (b) August 2018 in cities of the GZB and Hanzhong (XA, XY, WN, BJ, TC and HZ represent the urban areas in Xi'an, Xianyang, Weinan, Baoji, Tongchuan and Hanzhong respectively).

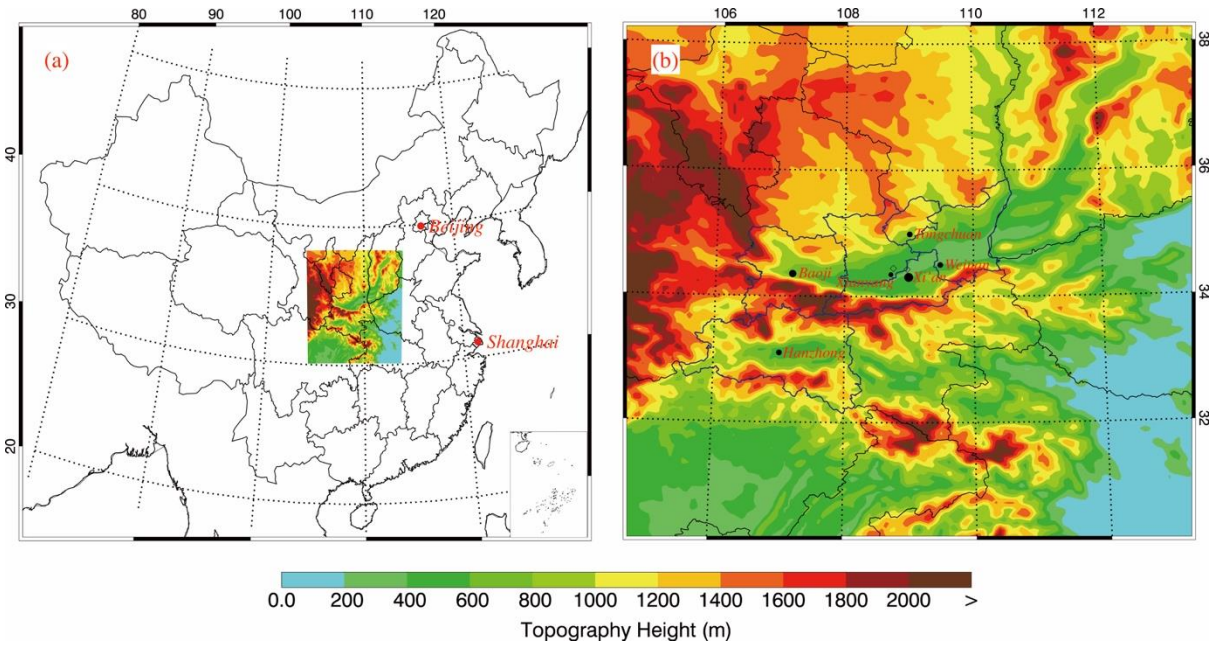

Figure 1 WRF-Chem simulation domain with topography. The filled black circles represent centers of cities with ambient monitoring sites and the size of circles denotes the number of ambient monitoring sites of cities. The diamond denotes the meteorological observation station. The areas surrounded by deep blue lines are focused in this study (GZB and Hanzhong city).

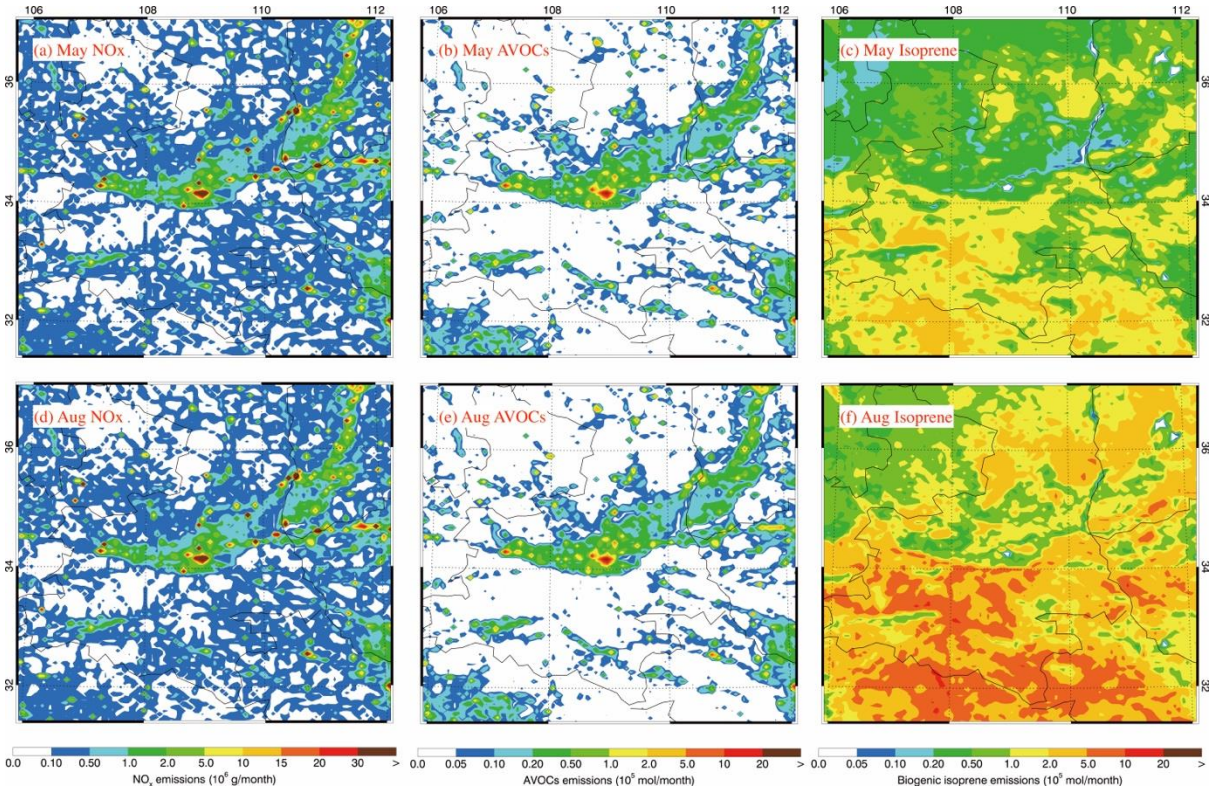

Figure 2 Spatial distribution of (a)/(d) anthropogenic NO_X, (b)/(e) anthropogenic VOCs, and (c)/(f) biogenic isoprene emission rates in May/August.

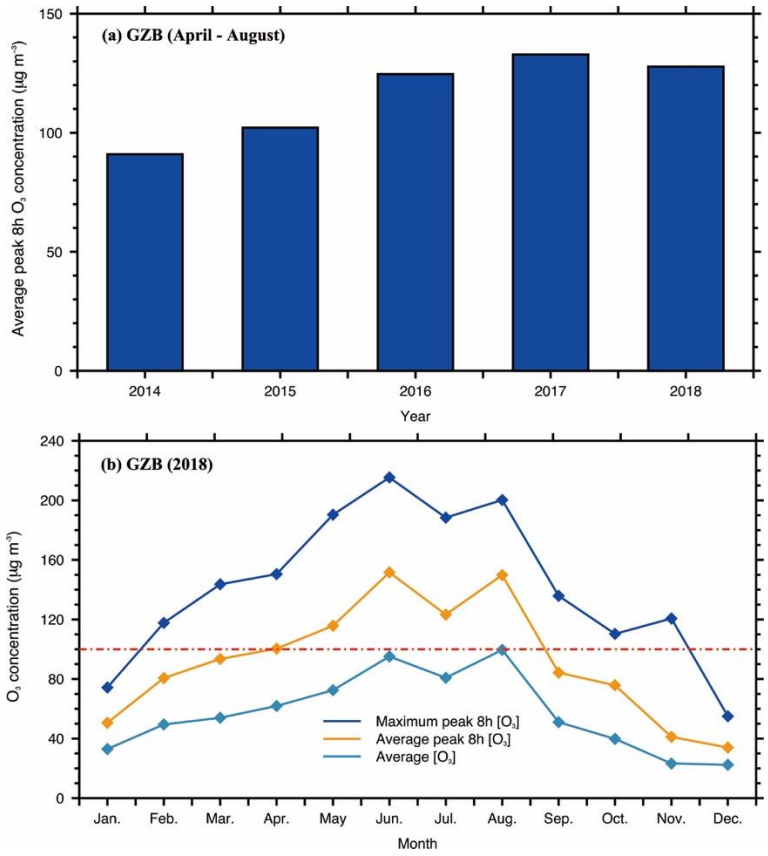

703

704

705 Figure 3 (a) trends of observed average peak 8-h [O_3] in warm seasons (from April to August) in the
706 GZB from 2014 to 2018, and (b) maximum peak 8-h [O_3] (dark blue line), average peak 8-h daily [O_3]
707 (light blue line) and monthly average [O_3] (yellow line) in 2018 in the GZB. The red line indicates the
708 first grade of National Ambient Air Quality Standards for average peak 8-h daily [O_3] in China.

709

710

711

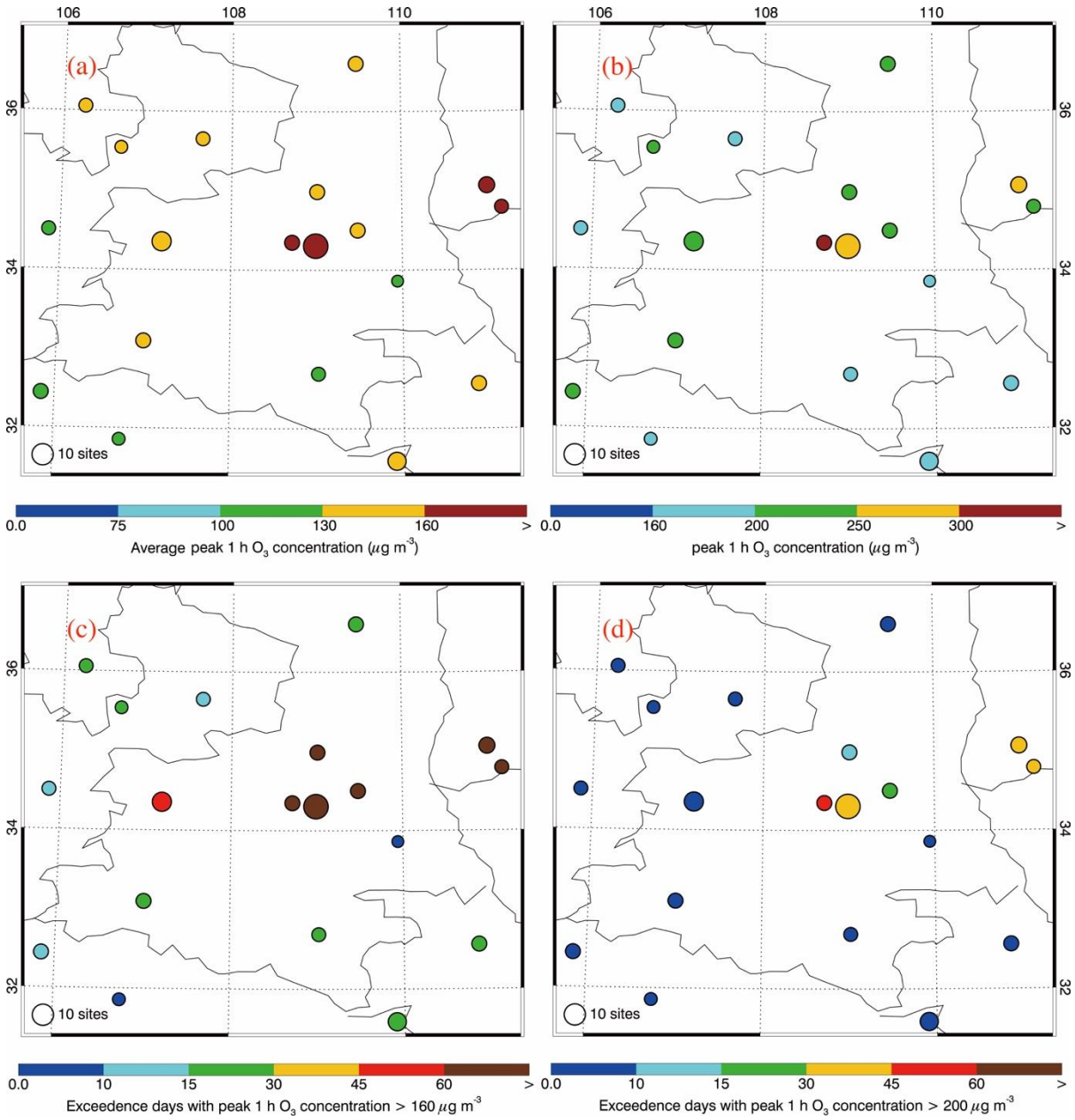

712

713

714 Figure 4 Distribution of observed (a) average daily peak 1-h [O_3], (b) maximum daily peak 1-h [O_3],
715 (c) days with the observed peak 1h [O_3] exceeding 160 μg m^{-3} and (d) days with the observed peak
716 1-h [O_3] exceeding 200 μg m^{-3} in the GZB and surrounding areas from April to August 2018.

717

718

719

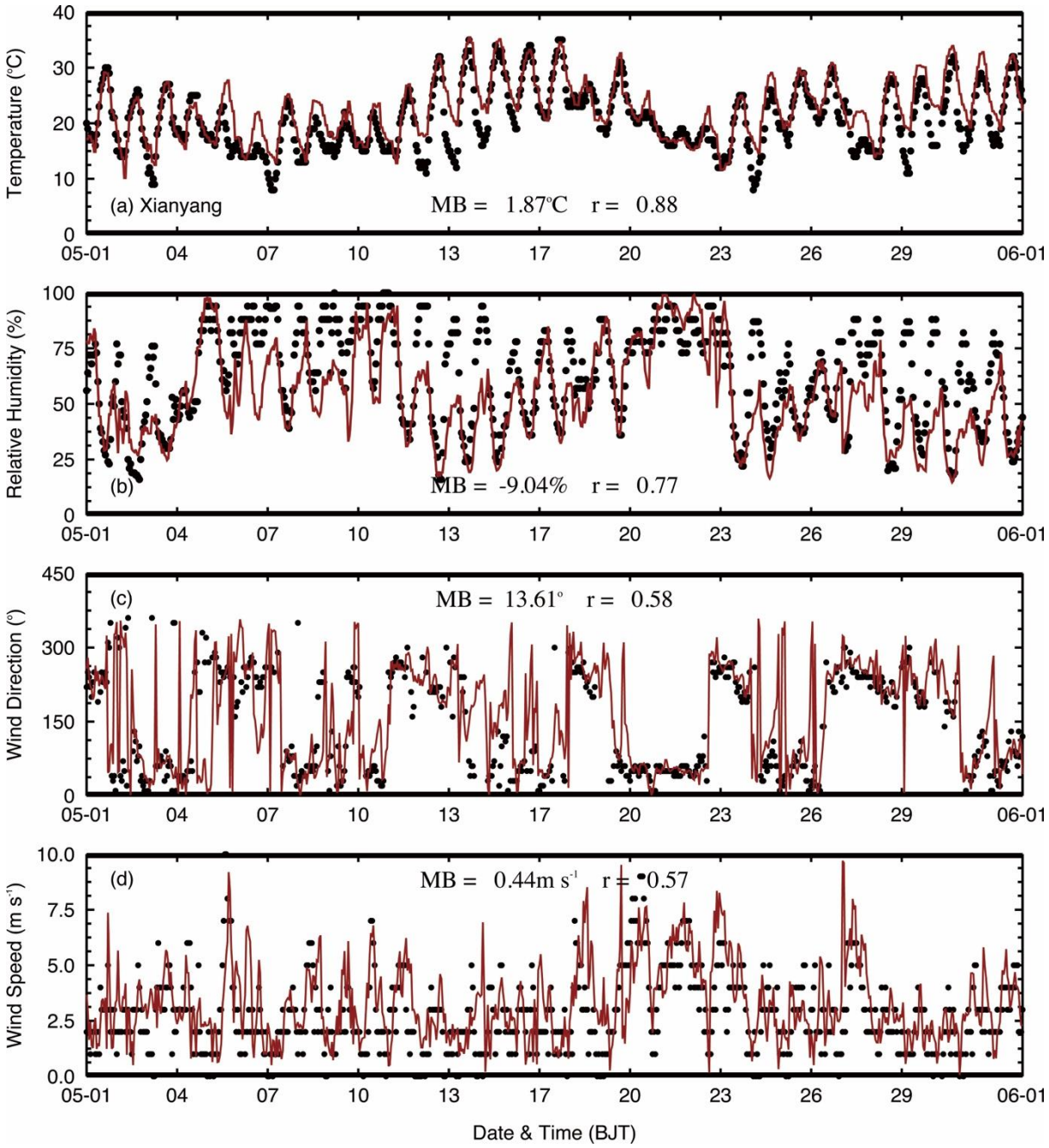

720

721

722 Figure 5 Temporal variations of predicted (red) and observed (black) (a) temperature at 2 m, (b)
723 relative humid at 2 m, (c) wind direction and (d) wind speed at 10 m at Xianyang meteorological
724 monitoring site in May 2018. The model performance statistic metrics of MB and R are also shown.

725

726

727

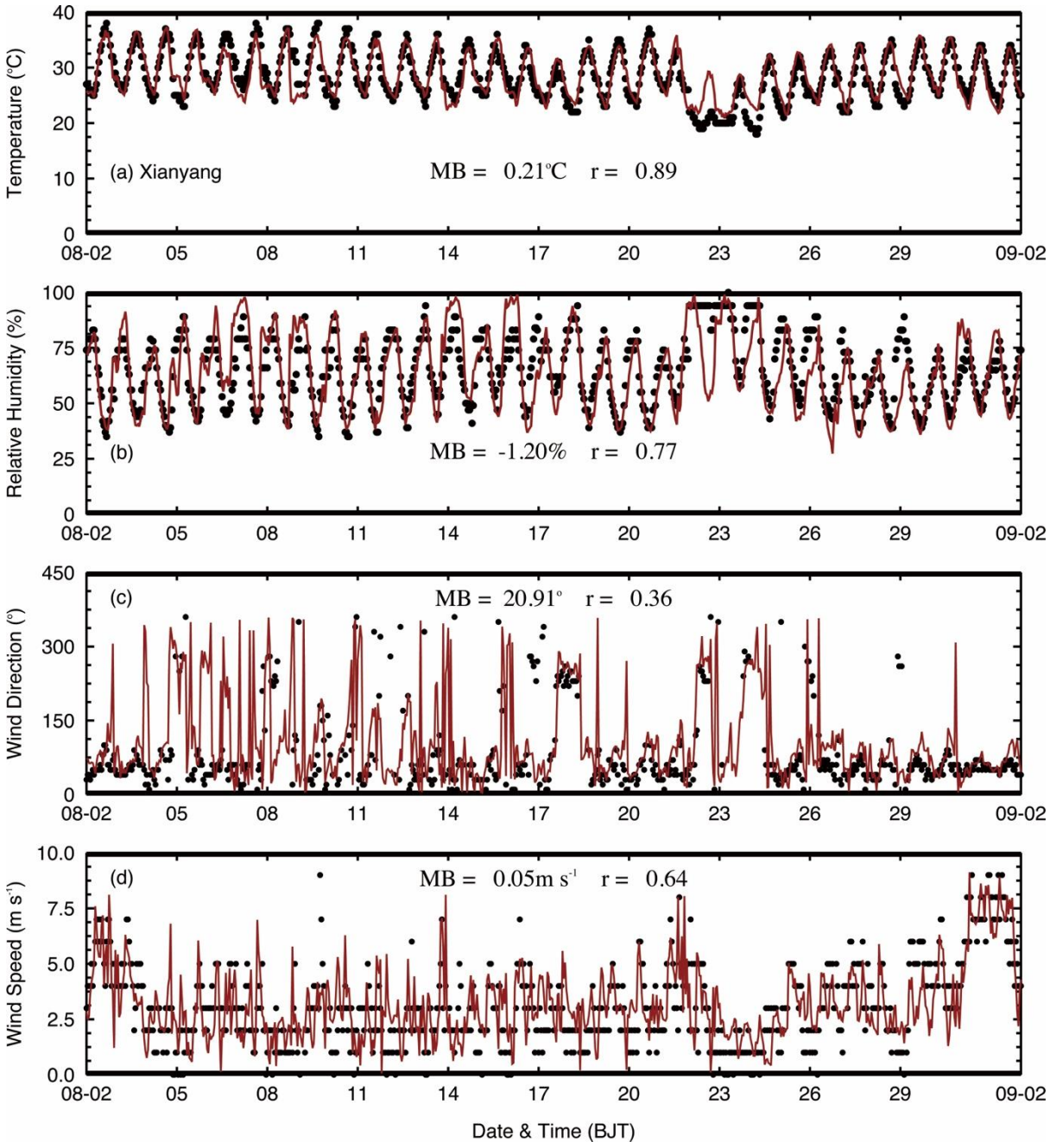

Figure 6 Same as Figure 5, but for August 2018.

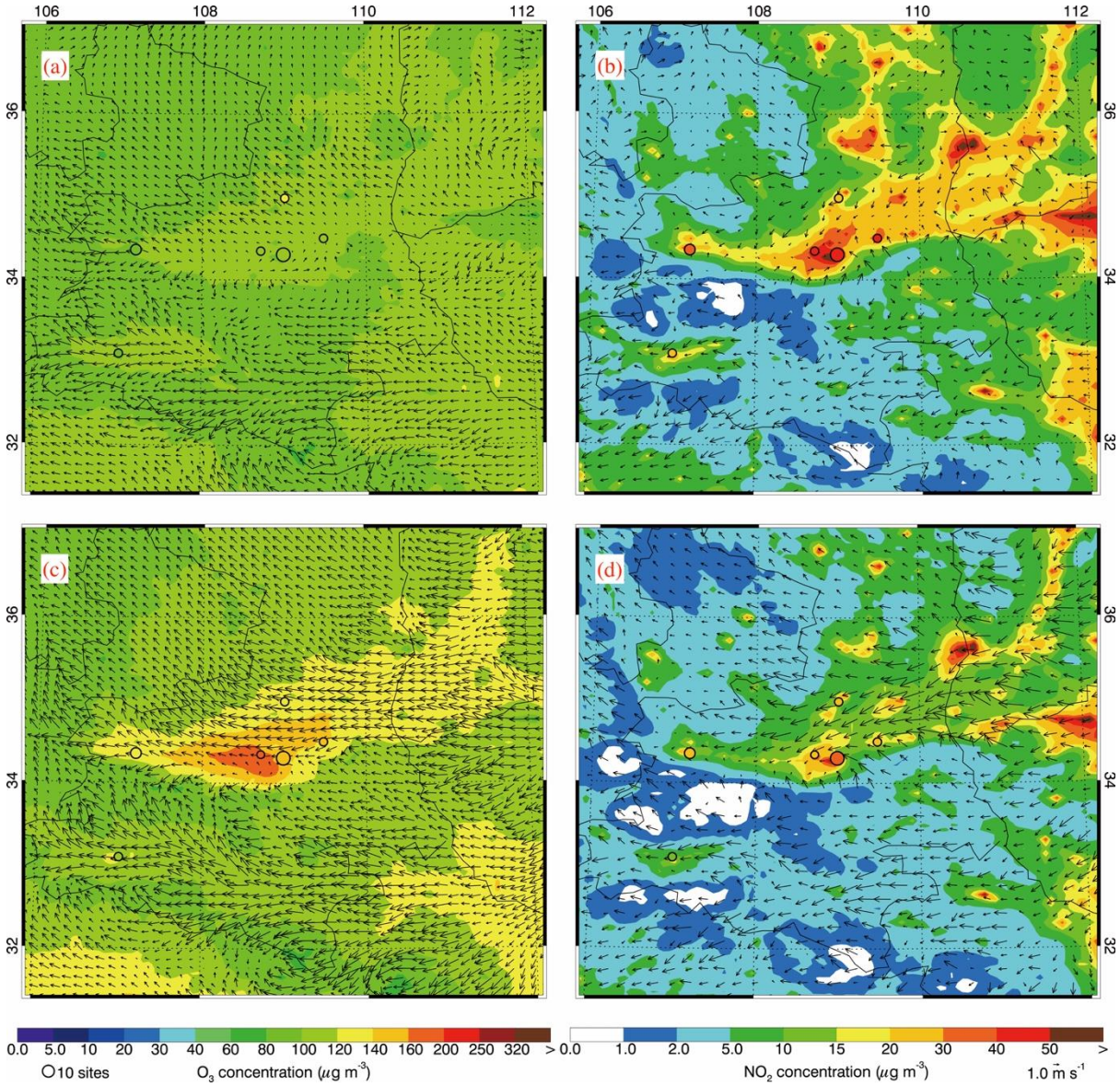

Figure 7 Pattern comparisons of simulated versus observed average (a)/(c) daily peak 8-h O_3 and (b)/(d) NO_2 concentrations in May/August 2018. Colored circles: O_3 observations; color contour: O_3 simulations; black arrows: simulated near-surface winds.

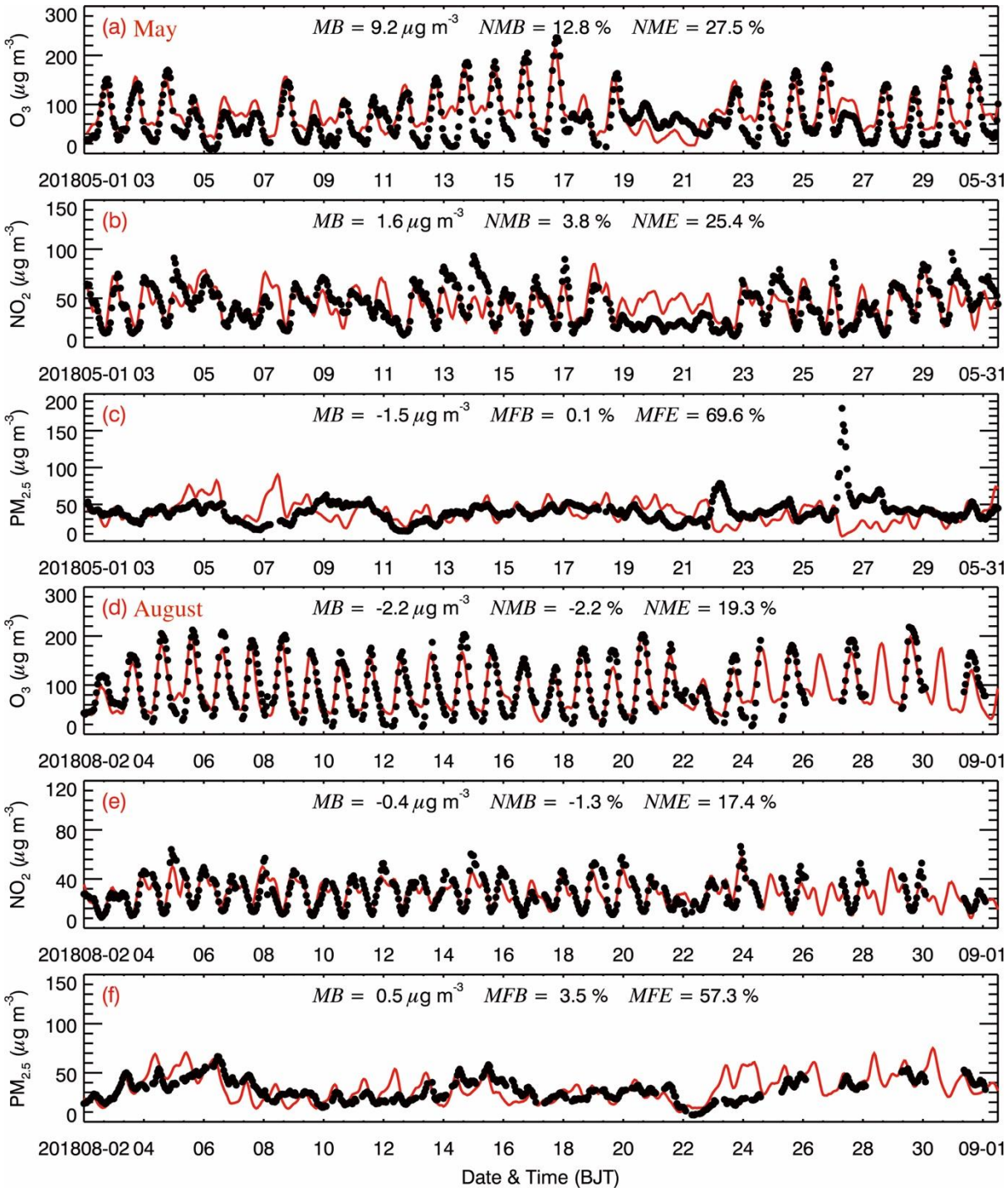

742

743

744 Figure 8 Diurnal profiles of measured (black dots) and predicted (red line) (a)/(d) O_3, (b)/(e) NO_2 and
745 (c)/(f) $PM_{2.5}$ concentrations averaged over all ambient monitoring stations in the GZB in May/August
746 2018.

747

748

749

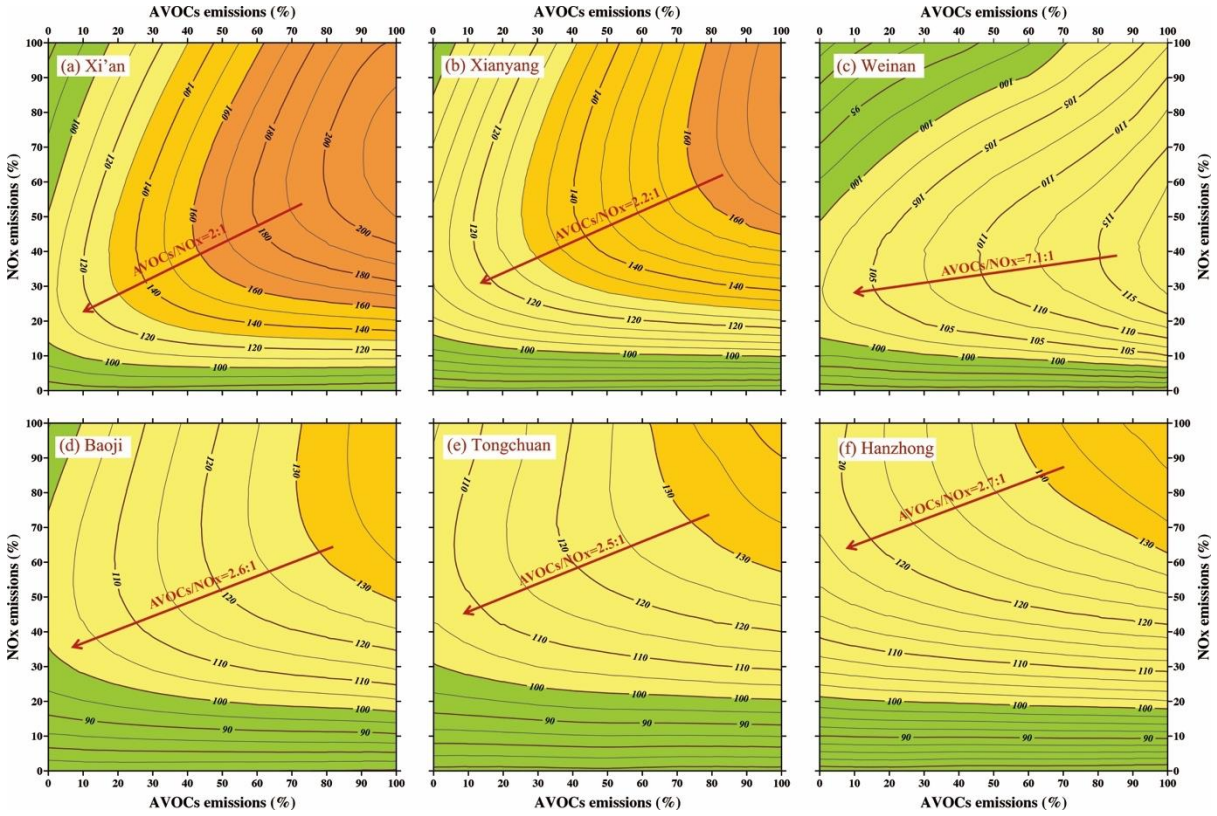

Figure 9 O_3 isopleth profiles (μg m^{-3} of average daily peak 8-h concentrations) in urban areas of (a) Xi'an, (b) Xianyang, (c) Weinan, (d) Baoji, (e) Tongchuan and (f) Hanzhong on 16 May 2018. The VOC-limited and NOx-limited regimes are separated by the red ridge lines.

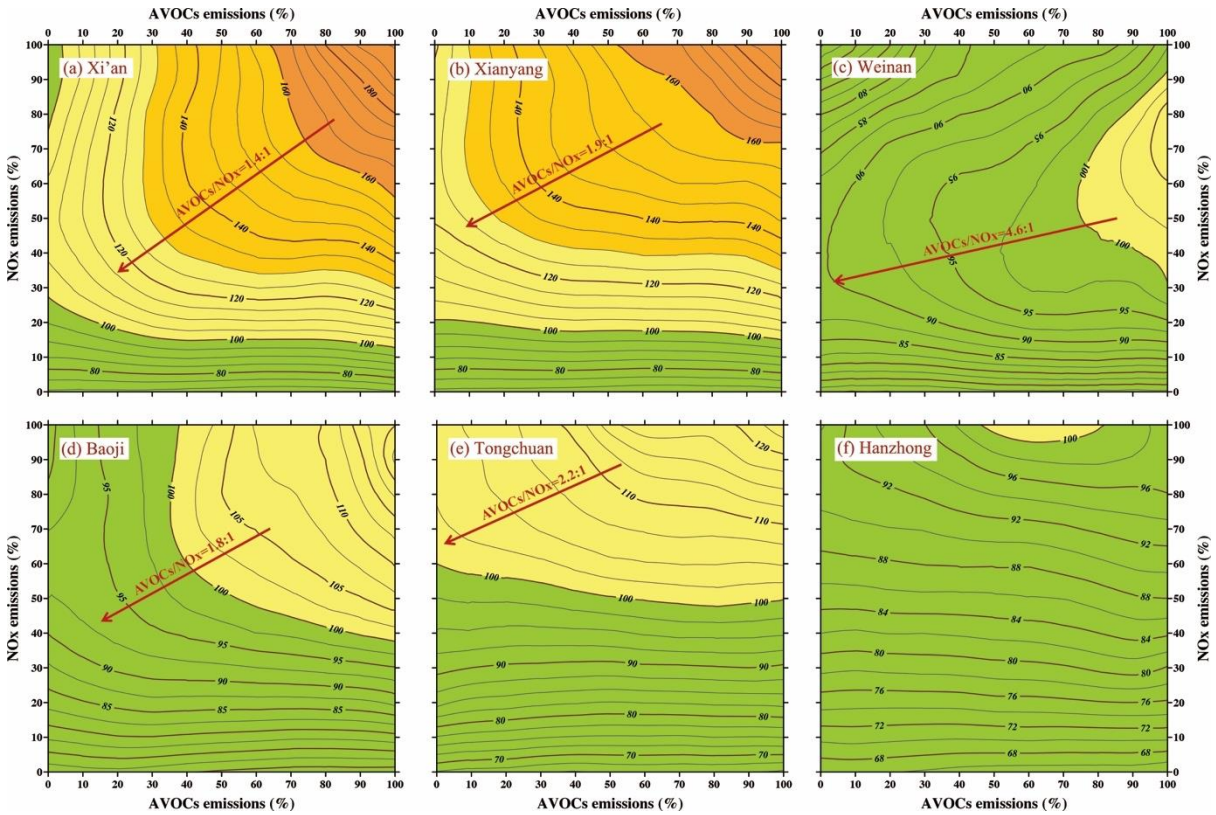

Figure 10 Same as Figure 9, but for 7 August 2018.

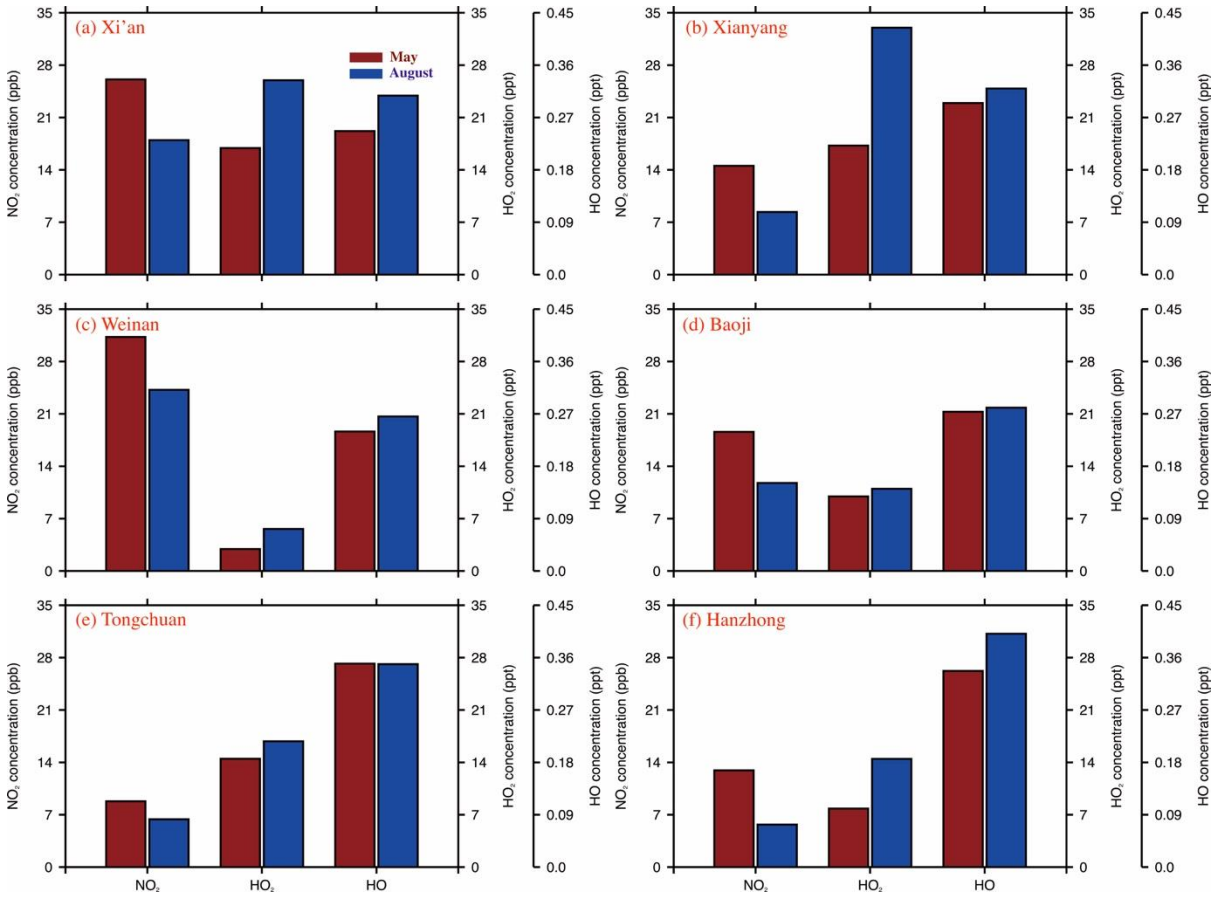

764

765

766 Figure 11 Average daytime NO_2, HO_2 and HO concentrations during springtime on 16 May 2018 and
767 7 August 2018 in urban areas of (a) Xi'an, (b) Xianyang, (c) Weinan, (d) Baoji, (e) Tongchuan and (f)
768 Hanzhong.

769

770

771

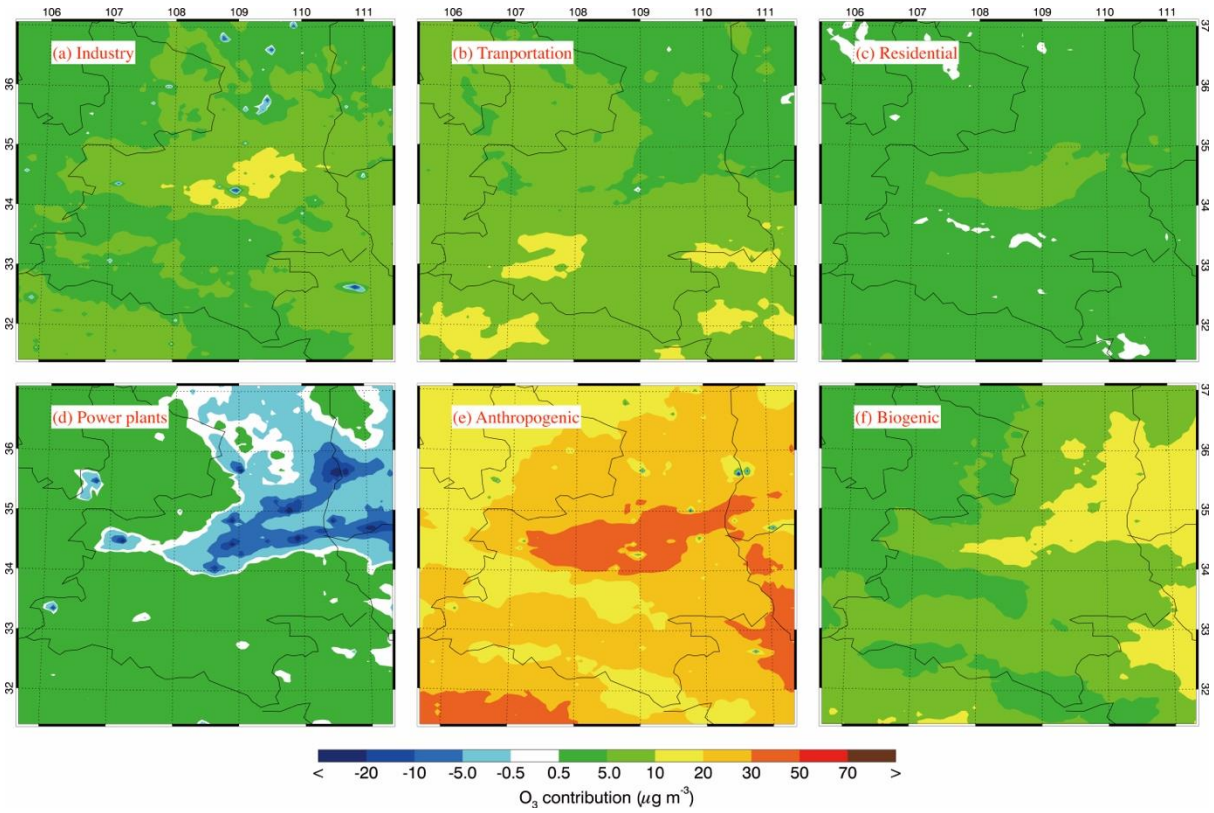

772

773

774 Figure 12 Distributions of the average peak 8-h O_3 contribution in May 2018 from (a) industry, (b)
775 transportation, (c) residential, (d) power plants, (e) total anthropogenic, and (f) biogenic sources.

776

777

778

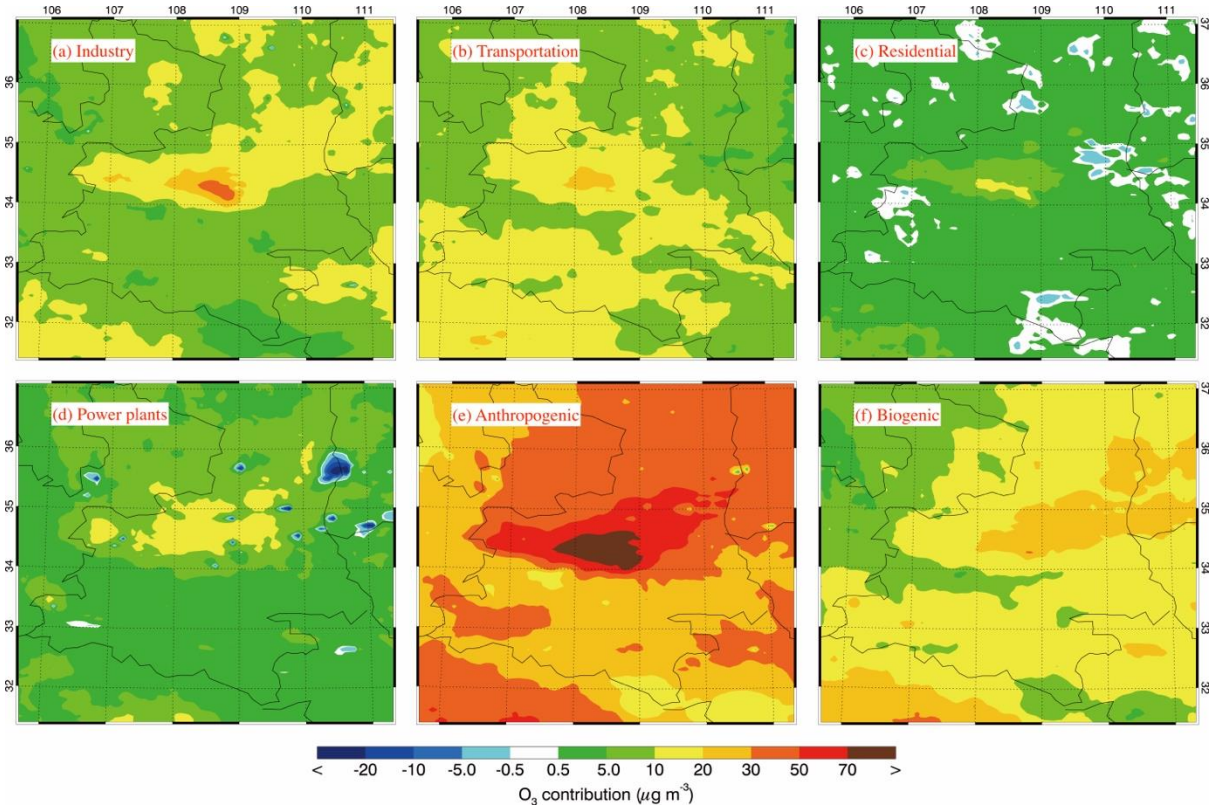

779

780

781 Figure 13 Same as Figure 12, but for August 2018.

782

783

784

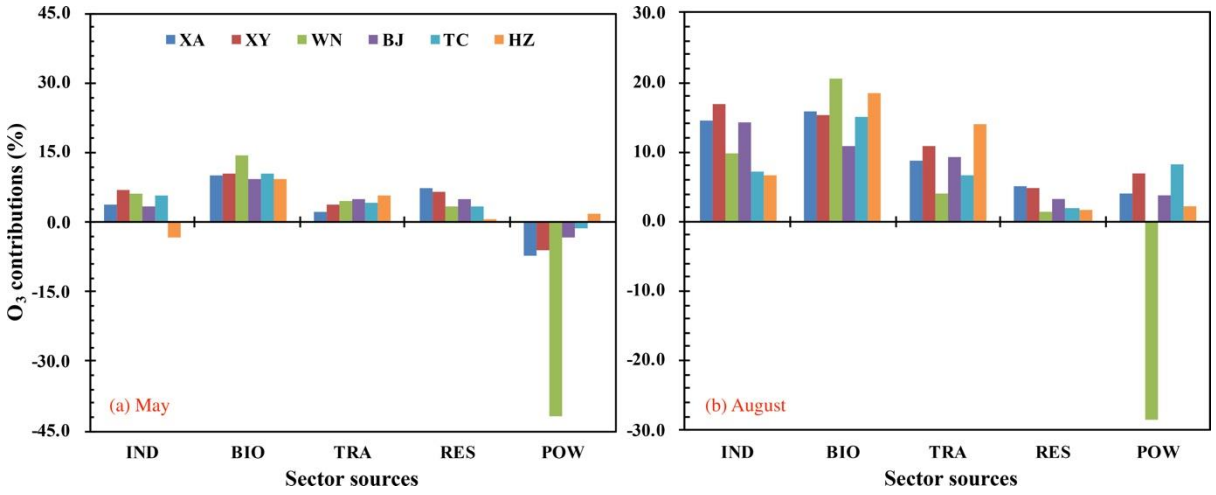

785

786

787 Figure 14 Average peak 8-h O_3 contributions from various sources in (a) May and (b) August 2018 in
788 cities of the GZB and Hanzhong (XA, XY, WN, BJ, TC and HZ represent the urban areas in Xi'an,
789 Xianyang, Weinan, Baoji, Tongchuan and Hanzhong respectively).

790

791